Advances in Aircraft and Spacecraft Science, *Vol. 11, No. 4 (2024) 313-329*
https://doi.org/10.12989/aas.2024.11.4.313

On the analysis of longitudinal fracture in functionally graded rods performing non-uniform rotational movement

Victor I. Rizov*

Department of Technical Mechanics, University of Architecture, Civil Engineering and Geodesy, 1 Chr. Smirnensky Blvd., 1046, Sofia, Bulgaria

(Received November 6, 2024, Revised December 20, 2024, Accepted January 2, 2025)

Abstract. Various components of mechanisms and devices that are extensively used in a variety of aerospace and aeronautical applications frequently perform different kinds of movement with acceleration. According to D'Alembert's principle, the acceleration induces forces of inertia that have to be taken into account when analyzing various problems in the area of strength, fracture, stability, durability, reliability, etc. of components of load-bearing engineering structures, machines, mechanisms and devices. Having in mind that functionally graded materials are widely applied for manufacturing of high performance structures in modern aerospace industry, analyzing fracture behaviour of functionally graded structural members represents a problem of the present day. The goal of this paper is to analyze longitudinal fracture in functionally graded rods which perform non-uniform rotational movement around a pinned support. Non-linear viscoelastic rods that are functionally graded along the thickness and length are considered. The problem of determination of the strain energy release rate (SERR) in rods with a longitudinal crack under the action of distributed forces of inertia induced by the normal and tangential acceleration is treated generally (in essence, this is a dynamic problem). The distribution of the forces of inertia in the rod is analyzed. An application of the general approach for solving a particular problem is presented. The solution is confirmed by the integral J. The influence of various parameters of the model is studied. For instance, the influence of the ratio of the values of material parameters on the upper and lower surface of the rotating beam on the SERR is studied in detail. It is found that the SERR is very sensitive with respect to these ratios. A practical application of the solution for determining the boundary value of the parameter involved in the rotation law and the boundary crack length is presented.

Keywords: forces of inertia; functionally graded rod; longitudinal fracture; non-uniform rotational movement; viscoelastic behaviour

1. Introduction

The numerous advantages provided by functionally graded materials are an important factor for enhancing the efficiency in many areas of up-to-date engineering including aerospace and aeronautical industry (Mahamood and Akinlabi 2017). This is due mainly to very good properties of these novel continuously inhomogeneous composite materials (Faleh *et al.* 2018, Gasik 2010, Hedia *et al.* 2014, Khaled Amara *et al.* 2016, Mahamood and Akinlabi 2017). These properties are attained by a favourable combination of the characteristics of the phases of functionally graded materials (Bouazza and Zenkour 2020, Civalek *et al.* 2021, Dastjerdi *et al.* 2020, Derbale *et al.*

*Corresponding author, Professor, E-mail: v_rizov_fhe@uacg.bg

http://www.techno-press.org/?journal=aas&subpage=7 ISSN: 2287-528X (Print), 2287-5271 (Online)

2021, El-Galy *et al.* 2019, Rizov and Altenbach 2019, Saiyathibrahim *et al.* 2016, Shrikantha and Gangadharan 2014). As known, usually, the functionally graded materials have two or more material phases which are mixed in a desired way during fabrication process (Akbaş *et al.* 2021, Ellali *et al.* 2022, Markworth *et al.* 1995, Miyamoto *et al.* 1999, Nemat-Allal *et al.* 2011, Rizov 2020, Toudehdehghan *et al.* 2017). The ratio of the phases may be varied within a broad range. The functionally graded materials have a smoothly changing microstructure along one or more directions which ensures a smooth change of their properties. Nowadays, the functionally graded composites are related to the most perspective engineering materials which rapidly replace pure (homogeneous) materials in a variety of applications mainly because the pure materials cannot provide the necessary mechanical properties that are able to sustain high stress levels during the lifetime of structures, outfits and machines (Atmane *et al.* 2016, Bouazza and Zenkour 2020, Bouazza *et al.* 2018, Khaled Amara *et al.* 2016, Mokhtar Ellali *et al.* 2022, Rizov and Altenbach 2022, Tokovyy and Ma 2017, Tokovyy and Ma 2019, Tokovyy 2019, Tokovyy and Ma 2021, Tokovyy 2023, Yıldırım and Akgöz 2024).

The increasing interest in use of functionally graded materials in aeronautics and aerospace requires development of approaches for accurate prediction, analysis and assessment of different aspects of the behaviour of these materials and structures under various loading conditions and influences. Thermal buckling characteristics of functionally graded plates subjected to combined action of thermal load and constant applied actuator voltage are investigated (Ellali *et al.* 2024). The thermo-mechanical material properties of plates are temperature dependent. Influence of several parameters on the critical buckling temperature is studied and discussed (Ellali *et al.* 2024). The vibration behaviour of functionally graded nanobeam under a hygrothermal environment is explored by a new higher-order methodology (Ellali *et al.* 2024). Different environmental conditions are considered. The nanobeam is resting on Winkler-Pasternak-type medium. The impact of various environmental factors, material properties and the elastic foundation is examined. The study contributes for understanding the free vibration behaviour of functionally graded nanobeams with hydrothermal effects (Ellali *et al.* 2024). An integral shear strain model is applied in studying vibration of functionally graded beams (Ellali *et al.* 2024). Power functions are used for presenting the change of the material properties along the beam thickness. Several power functions (linear, quadratic, cubic and inverse quadratic) are applied (Ellali *et al.* 2024). The wave propagation in functionally graded plates is analyzed by a new integral inverse shear model with temperature-dependent material properties (Ellali *et al.* 2023). The properties change is treated by power functions of the plate thickness. General formulas of wave propagation are obtained. The influence of the volume fractions on the wave propagation in functionally graded plates is investigated (Ellali *et al.* 2023).

One of the main problems concerning failure behaviour of the functionally graded structures is their fracture in the conditions of dynamic loading. The strong interest towards dynamic fracture behaviour is due to the fact that many components of mechanisms, devices and structures used in aerospace and aeronautics perform different kinds of motion with acceleration. As known, acceleration induces inertia forces that have to be taken into account when dealing with issues like analysis of strength and fracture. A particular interest represents analysis of longitudinal fracture in functionally graded components and members under dynamic loading. This is due to the frequent application of a technology for manufacturing of functionally graded components that essentially presents building-up layer-by-layer which creates conditions for origin of longitudinal cracks (Mahamood and Akinlabi 2017). These cracks usually have rather negative effect on the strength, reliability and safety (Dolgov 2005, Dolgov 2016, Dowling 2013, Rizov and Altenbach 2019,

Rizov 2022, Rizov 2024). The longitudinal cracks may cause severe disturbances of the functioning of mechanisms and devices and even may lead to failure with catastrophic consequences including lose of human lives. These facts indicate that analyzing of longitudinal fracture in functionally graded components and members which perform motion with acceleration can be regarded as an important up-to-date research task that has both theoretical and practical meaning.

The aforesaid motivates the author to carry-out the research described in this paper. In particular, a rod performing non-uniform rotational movement around a pinned support is considered. The rod hosts a longitudinal crack. The main aim is to analyze the SERR with taking into account the distributed forces of inertia induced by the normal and tangential accelerations. The deadweight is also taken into account. The analysis incorporates such phenomena as double material inhomogeneity (the rod is functionally graded along thickness and length) and non-linear viscoelastic behaviour. The rods under consideration are long, i.e., their length to thickness ratio is high (in fact, this assumption is the basic limitation of the study). First, general treatment of the problem is presented. The treatment includes a detailed analysis of the distribution of forces of inertia in a rod with a longitudinal crack. Then general approach for deriving the SERR is developed. The general approach is used for solving a particular problem. The solution is confirmed by the integral *J*. The effects of various parameters of the dynamic model of the rod on the SERR are investigated. Based on the results of this investigation, numerous graphs are presented. The solution of the SERR derived is applied also for assessing the safety of a rod in which a longitudinal crack is observed during lifetime.

2. General approach

The subject of study in the this paper is the rod, B_1B_3, displayed in Fig. 1. The rod performs rotation around the pinned support in point, B_1. The law of rotation is a continuous function of time presented by the next formula.

$$\phi = \phi(t), \tag{1}$$

where ϕ is the angle of rotation (displayed in Fig. 1), t is time.

In portion, B_2B_3, the rod hosts a longitudinal crack. The thicknesses of the two arms of this crack are h_1 and h_2 as displayed in Fig. 1. Portion, B_1B_2, of the rod is intact.

The angular velocity, ω, and the angular acceleration, α, of the rod can be found via the next two formulas.

$$\omega = \frac{d\phi}{dt}, \tag{2}$$

$$\alpha = \frac{d^2\phi}{dt^2}. \tag{3}$$

The normal and the tangential accelerations, a_n and a_τ, in a given point of the rod which are needed for determining the intensities of the distributed forces of inertia are derived by formulas (4) and (5), respectively.

$$a_n = \omega^2 x, \tag{4}$$

$$a_\tau = \alpha x, \tag{5}$$

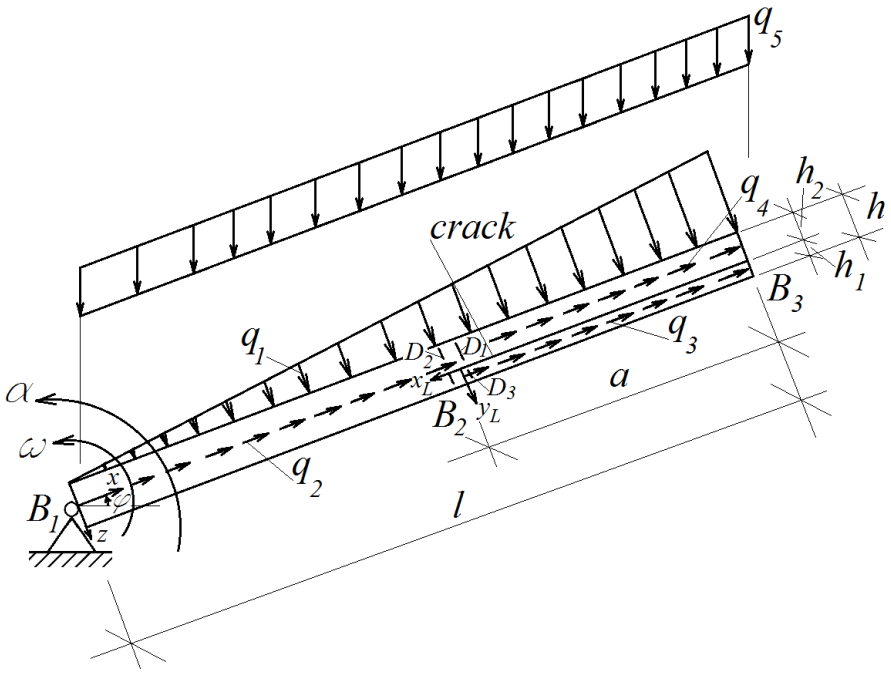

Fig. 1 Geometry and loading of a rod performing non-uniform rotation

where

$$0 \leq x \leq l. \tag{6}$$

In the above formulas, x is the longitudinal axis of the rod, l is the rod length (x and l are displayed in Fig. 1).

The density of the transversal forces of inertia, q_1, is calculated as written below.

$$q_1 = m_d a_\tau, \tag{7}$$

where m_d is the mass per unit length of the rod. The latter is found by using formula (8), i.e.

$$m_d = \frac{m}{l}, \tag{8}$$

where m is the mass of the rod. The distribution of q_1 is displayed in Fig. 1.

The density of the longitudinal forces of inertia, q_2, in the intact portion of the rod is determined by the next formula.

$$q_2 = m_d a_n. \tag{9}$$

The density of the longitudinal forces of inertia, q_3, in the crack arm of thickness, h_1, is found by formula (10), i.e.

$$q_3 = m_{dh1} a_n, \tag{10}$$

where the mass per unit length, m_{dh1}, is

$$m_{dh1} = m_d \frac{h_1}{h}. \tag{11}$$

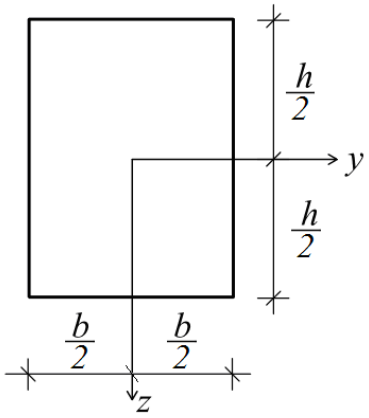

Fig. 2 Rod cross-section

Similarly, the density of the longitudinal forces of inertia, q_4, in the crack arm of thickness, h_2, is

$$q_4 = m_{dh1} a_n, \tag{12}$$

where

$$m_{dh1} = m_d \frac{h_2}{h}. \tag{13}$$

Formulas (10) and (12) hold for

$$l - a \leq x \leq l, \tag{14}$$

where a is the length of the longitudinal crack (Fig. 1). The distributions of q_3 and q_4 are displayed schematically in Fig. 1.

The distributed deadweight, q_5, of the rod is

$$q_5 = m_d g, \tag{15}$$

where g is the acceleration of gravity. The distribution of q_4 can be seen in Fig. 1.

Our basic aim is to derive the SERR, G, for the longitudinal crack in the rod in Fig. 1 under the action of the forces of inertia and the deadweight. For achieving of this aim we apply formula (16), i.e.

$$G = \frac{dU^*}{dA}, \tag{16}$$

where U^* is the complementary strain energy in the rod, A is the crack area. Formula (16) is transformed as

$$G = \frac{dU^*}{bda}, \tag{17}$$

because

$$dA = bda, \tag{18}$$

where b is the rod width (the rod cross-section is displayed in Fig. 2).

The complementary strain energy in the rod is presented as given below.

$$U^{*} = U^{*}_{B1B2} + U^{*}_{B2B3h1} + U^{*}_{B2B3h2}, \tag{19}$$

where the subscripts, B_1B_2, $B_2B_3h_1$, and $B_2B_3h_2$, refer to the intact portion of the rod and the crack arms of thicknesses, h_1 and h_2, respectively. The quantities involved in (19) can be calculated by applying the next three formulas.

$$U^{*}_{B1B2} = \int_0^{l-a}\left(b\int_{-\frac{h}{2}}^{\frac{h}{2}} u^{*}_{0B1B2}\,dz\right)dx, \tag{20}$$

$$U^{*}_{B2B3h1} = \int_{l-a}^{l}\left(b\int_{-\frac{h_1}{2}}^{\frac{h_1}{2}} u^{*}_{0B2B3h1}\,dz_1\right)dx, \tag{21}$$

$$U^{*}_{B2B3h2} = \int_{l-a}^{l}\left(b\int_{-\frac{h_2}{2}}^{\frac{h_2}{2}} u^{*}_{0B2B3h2}\,dz_2\right)dx, \tag{22}$$

where z, z_1 and z_2 are the vertical centric axes of the cross-sections of the intact portion of the rod and the crack arms of thicknesses, h_1 and h_2, respectively. The quantities, u^{*}_{0B1B2}, $u^{*}_{0B2B3h1}$ and $u^{*}_{0B2B3h2}$, in formulas (20), (21) and (22) represent the complementary strain energy densities in the intact portion of the rod and the crack arms of thicknesses, h_1 and h_2, respectively. These quantities can be obtained by the formulas given below, i.e.

$$u^{*}_{0B1B2} = \sigma\varepsilon - \int \sigma d\varepsilon, \tag{23}$$

$$u^{*}_{0B2B3h1} = \sigma_{B2B3h1}\varepsilon_{B2B3h1} - \int \sigma_{B2B3h1} d\varepsilon_{B2B3h1}, \tag{24}$$

$$u^{*}_{0B2B3h2} = \sigma_{B2B3h2}\varepsilon_{B2B3h2} - \int \sigma_{B2B3h2} d\varepsilon_{B2B3h2}, \tag{25}$$

where σ and ε are the stress and strain in the intact portion of the rod, σ_{B2B3h1} and ε_{B2B3h1}, and σ_{B2B3h2} and ε_{B2B3h2}, are the stress and the strain in the crack arms of thicknesses, h_1 and h_2, respectively.

In order to proceed further, we need a constitutive law. In this paper, the stresses and strains in the rod are related by a constitutive law representing a non-linear dependence between stresses, strains and time because the material has non-linear viscoelastic behaviour. This law is written as given below (Varbanov *et al.* 1992).

$$\sigma(\varepsilon, t) = s_1 s_2, \tag{26}$$

where

$$s_1 = s_1(\varepsilon) \tag{27}$$

and

$$s_2 = s_2(t). \tag{28}$$

Here, $s_1(\varepsilon)$ and $s_2(t)$ are non-linear functions of the strain and time, respectively. It should by noted that the material parameters involved in (27) and (28) are continuous functions of both longitudinal and transversal coordinates, x and z, where

$$0 \le x \le l \tag{29}$$

and

$$-\frac{h}{2} \le z \le \frac{h}{2}, \tag{30}$$

since the material is functionally graded along the length and thickness of the rod.

In order to determine the SERR by applying formula (17), we have to analyze the variation of the strains along the rod thickness. This variation represents a function of two parameters (the rod curvature, κ, and the neutral axis coordinate, z_n) as given below.

$$\varepsilon = \kappa(z - z_n). \tag{31}$$

The curvature and the neutral axis coordinate of an arbitrary cross-section of the intact portion of the rod are determined from the next two equations.

$$N = b\int_{-\frac{h}{2}}^{\frac{h}{2}} \sigma dz \tag{32}$$

and

$$M = b\int_{-\frac{h}{2}}^{\frac{h}{2}} \sigma z dz, \tag{33}$$

where N and M are the axial force and the bending moment in the rod cross-section induced by the forces of inertia and the deadweight. The stress, σ, that is involved in (32) and (33) is related to ε through (26).

In the crack arm of thickness, h_1, the variation of ε_{B2B3h1} is given be the next formula.

$$\varepsilon_{B2B1h1} = \kappa_1(z_1 - z_{1n}), \tag{34}$$

where

$$-\frac{h_1}{2} \le z_1 \le \frac{h_1}{2}. \tag{35}$$

The two parameters, κ_1 and z_{1n}, involved (34) for an arbitrary cross-section are determined from the following equations:

$$N_{B2B3h1} = b\int_{-\frac{h_1}{2}}^{\frac{h_1}{2}} \sigma_{B2B3h1} dz_1 \tag{36}$$

and

$$M_{B2B3h1} = b\int_{-\frac{h_1}{2}}^{\frac{h_1}{2}} \sigma_{B2B3h1} z_1 dz_1, \tag{37}$$

where N_{B2B3h1} and M_{B2B3h1} are the axial force and the bending moment in the cross-section induced by the forces of inertia and the deadweight acting on the crack arm under consideration.

The parameters, κ_2 and z_{2n}, of the variation of ε_{B2B3h2} along the thickness, h_2, of an arbitrary cross-section are determined by equation similar to (36) and (37), i.e.

$$N_{B2B3h2} = b\int_{-\frac{h_2}{2}}^{\frac{h_2}{2}} \sigma_{B2B3h2} dz_2 \tag{38}$$

and

$$M_{B2B3h2} = b\int_{-\frac{h_2}{2}}^{\frac{h_2}{2}} \sigma_{B2B3h2} z_2 dz_2, \tag{39}$$

where the axial force, N_{B2B3h2}, and the bending moment, M_{B2B3h2}, are induced by the forces of inertia and the deadweight acting on the crack arm of thickness, h_2.

It should be noted that Eqs. (34), (36), (37), (38) and (39) hold for beam portion, B_2B_3, i.e., for

$$l - a \leq x \leq l. \tag{40}$$

At the end, the SERR is derived by inserting of (23), (24) and (25) in formula (17). The integration is performed by the MatLab.

3. Application of the general approach

This section of the paper is devoted to obtaining of concrete results by applying the general approach. The rotation of the rod obeys the law presented in formula (41).

$$\phi(t) = \beta t^2, \tag{41}$$

where β is a parameter.

The angular velocity and the angular acceleration are found by applying formulas (2), (3) and (41). The result is given below.

$$\omega = 2\beta t, \tag{42}$$

$$\alpha = 2\beta. \tag{43}$$

The densities of the forces of inertia derived by using formulas (4), (5), (7), (9), (12), (42) and (43) are written as follows

$$q_1 = 2m_d\beta x, \tag{44}$$

$$q_2 = 4m_d\beta^2 t^2 x, \tag{45}$$

$$q_3 = 4m_{dh1}\beta^2 t^2 x, \tag{46}$$

$$q_4 = 4m_{dh2}\beta^2 t^2 x. \tag{47}$$

The non-linear functions, $s_1(\varepsilon)$ and $s_2(t)$, involved in the constitutive law (26) are given below (Varbanov *et al.* 1992).

$$s_1(\varepsilon) = H_{\ 1}\varepsilon - H_{\ 2}\varepsilon^n - H_3\varepsilon^r \tag{48}$$

and

$$s_2(t) = \frac{1}{1+ln(1+\delta t^{\lambda})}. \tag{49}$$

Here, H_1, H_2, H_3, n, r, δ and λ are parameters.

As mentioned above, the rod is functionally graded along the length and thickness. Therefore the parameters involved in (48) and (49) are continuously distributed along the length and thickness of the rod. These distributions obey the laws presented in the next formulas.

$$H_1 = H_{1up} + \frac{H_{1lw}-H_{1up}}{h^{\rho_1}}\left(\frac{h}{2}+z\right)^{\rho_1}, \tag{50}$$

$$H_2 = H_{2up} + \frac{H_{2lw}-H_{2up}}{h^{\rho_2}}\left(\frac{h}{2}+z\right)^{\rho_2}, \tag{51}$$

$$H_3 = H_{3up} + \frac{H_{3lw}-H_{3up}}{h^{\rho_3}}\left(\frac{h}{2}+z\right)^{\rho_3}, \tag{52}$$

$$n = n_{up} + \frac{n_{lw}-n_{up}}{h^{\rho_4}}\left(\frac{h}{2}+z\right)^{\rho_4}, \tag{53}$$

$$r = r_{up} + \frac{r_{lw}-r_{up}}{h^{\rho_5}}\left(\frac{h}{2}+z\right)^{\rho_5}, \tag{54}$$

$$\delta = \delta_{up} + \frac{\delta_{lw}-\delta_{up}}{h^{\rho_6}}\left(\frac{h}{2}+z\right)^{\rho_6}, \tag{55}$$

$$\lambda = \lambda_{up} + \frac{\lambda_{lw}-\lambda_{up}}{h^{\rho_7}}\left(\frac{h}{2}+z\right)^{\rho_7}, \tag{56}$$

$$-\frac{h}{2} \le z \le \frac{h}{2}, \tag{57}$$

where the subscripts, up and lw, refer to the upper and lower surface of the rod, respectively, ρ_i, where $i = 1,2,\ldots,7$, are parameters.

The distributions along the rod length obey of the laws given below.

$$H_{1up} = H_{1upB1} + \frac{H_{1upB3}-H_{1upB1}}{l^{\mu_1}}x^{\mu_1}, \tag{58}$$

$$H_{1lw} = H_{1lwB1} + \frac{H_{1lwB3}-H_{1lwB1}}{l^{\mu_2}}x^{\mu_2}, \tag{59}$$

$$H_{2up} = H_{2upB1} + \frac{H_{2upB3}-H_{2upB1}}{l^{\mu_3}}x^{\mu_3}, \tag{60}$$

$$H_{2lw} = H_{2lwB1} + \frac{H_{2lwB3}-H_{2lwB1}}{l^{\mu_4}}x^{\mu_4}, \tag{61}$$

$$H_{3up} = H_{3upB1} + \frac{H_{3upB3}-H_{3upB1}}{l^{\mu_5}}x^{\mu_5}, \tag{62}$$

$$H_{3lw} = H_{3lwB1} + \frac{H_{3lwB3}-H_{3lwB1}}{l^{\mu_6}}x^{\mu_6}, \tag{63}$$

$$n_{up} = n_{upB1} + \frac{n_{upB3}-n_{upB1}}{l^{\mu_7}}x^{\mu_7}, \tag{64}$$

$$n_{lw} = n_{lwB1} + \frac{n_{lwB3}-n_{lwB1}}{l^{\mu_8}}x^{\mu_8}, \tag{65}$$

$$r_{up} = r_{upB1} + \frac{r_{upB3}-r_{upB1}}{l^{\mu_9}}x^{\mu_9}, \tag{66}$$

$$r_{lw} = r_{lwB1} + \frac{r_{lwB3}-r_{lwB1}}{l^{\mu_{10}}}x^{\mu_{10}}, \tag{67}$$

$$\delta_{up} = \delta_{upB1} + \frac{\delta_{upB3}-\delta_{upB1}}{l^{\mu_{11}}}x^{\mu_{11}}, \tag{68}$$

$$\delta_{lw} = \delta_{lwB1} + \frac{\delta_{lwB3}-\delta_{lwB1}}{l^{\mu_{12}}}x^{\mu_{12}}, \tag{69}$$

$$\lambda_{up} = \lambda_{upB1} + \frac{\lambda_{upB3}-\lambda_{upB1}}{l^{\mu_{13}}}x^{\mu_{13}}, \tag{70}$$

$$\lambda_{lw} = \lambda_{lwB1} + \frac{\lambda_{lwB3}-\lambda_{lwB1}}{l^{\mu_{14}}}x^{\mu_{14}}, \tag{71}$$

$$0 \le x \le l, \tag{72}$$

where subscripts, B_1 and B_3, refer to the end sections of the rod, μ_i, where $i = 1,2,\ldots,14$, are parameters.

Formulas (73) and (74) are used for determining the axial force and the bending moment that are involved in Eqs. (32) and (33).

$$N = 2m_d\beta^2t^2x(l-x) + 2m_d\beta^2t^2l(l-x) - m_dg(l-x)\sin\phi, \tag{73}$$

$$M = \frac{1}{3}m_d\beta x(l-x)^2 + \frac{2}{3}m_d\beta l(l-x)^2 + \frac{1}{2}m_dg(l-x)^2\cos\phi. \tag{74}$$

Then Eqs. (32) and (33) are solved for κ and z_n by the MatLab.

The axial force and the bending moment involved in Eqs. (36) and (37) are obtained by formulas (75) and (76), i.e.

$$N_{B2B3h1} = 2m_{dh1}\beta^2t^2x(l-x) + 2m_{dh1}\beta^2t^2l(l-x) - m_{dh1}g(l-x)\sin\phi, \tag{75}$$

$$M_{B2B3h1} = \frac{1}{3}m_{dh1}\beta x(l-x)^2 + \frac{2}{3}m_{dh1}\beta l(l-x)^2 + \frac{1}{2}m_{dh1}g(l-x)^2\cos\phi. \tag{76}$$

After that, the MatLab is used for determining κ_1 and z_{1n} from (36) and (37).

The quantities, κ_2 and z_{2n}, are found from equations (38) and (39) by the MatLab. The axial force and the bending moment involved in Eqs. (38) and (39) are derived by formulas (77) and (78), i.e.

$$N_{B2B3h2} = 2m_{dh2}\beta^2t^2x(l-x) + 2m_{dh2}\beta^2t^2l(l-x) - m_{dh2}g(l-x)\sin\phi, \tag{77}$$

$$M_{B2B3h2} = \frac{1}{3}m_{dh2}\beta x(l-x)^2 + \frac{2}{3}m_{dh2}\beta l(l-x)^2 + \frac{1}{2}m_{dh2}g(l-x)^2\cos\phi. \tag{78}$$

Finally, after substituting of the complementary strain energy in (17), the SERR is determined by the MatLab.

The SERR is checked by the integral J (Broek 1986). The J is solved by formula (79).

$$J_D = J_{D1} + J_{D2} + J_{D3}, \tag{79}$$

where the subscripts, D_1, D_2 and D_3, refer to the parts of the integration contour, $D_1D_2D_3$, displayed in Fig. 1. The quantities involved in (79) are

$$J_{D1} = \int \left[u_{0D1}\cos\alpha_{D1} - \left(p_{xLD1}\frac{\partial u_{D1}}{\partial x_L} + p_{yLD1}\frac{\partial v_{D1}}{\partial x_L}\right)\right]d\psi_1, \tag{80}$$

$$J_{D2} = \int \left[u_{0D2}\cos\alpha_{D2} - \left(p_{xLD2}\frac{\partial u_{D2}}{\partial x_L} + p_{yLD2}\frac{\partial v_{D2}}{\partial x_L}\right)\right]d\psi_2, \tag{81}$$

$$J_{D3} = \int \left[u_{0D3}\cos\alpha_{D3} - \left(p_{xLD3}\frac{\partial u_{D3}}{\partial x_L} + p_{yLD3}\frac{\partial v_D}{\partial x_L}\right)\right]d\psi_3. \tag{82}$$

Formulas (83)-(88) are used for obtaining the components of (80).

$$u_{0D1} = \int \sigma_{B2B3h2}d\varepsilon_{B2B3h2}, \tag{83}$$

$$\alpha_{D1} = -1, \tag{84}$$

$$p_{xLD1} = -\sigma_{B2B3h2}, \tag{85}$$

$$\frac{\partial u_{D1}}{\partial x_L} = \varepsilon_{B2B3h2}, \tag{86}$$

$$p_{yLD1} = 0, \tag{87}$$

$$d\psi_1 = -dz_2. \tag{88}$$

The axes, x_L and y_L, are displayed in Fig. 1.

The components of (81) are found by formulas (89)-(94).

$$u_{0D2} = \int \sigma d\varepsilon, \tag{89}$$

$$\alpha_{D2} = 1, \tag{90}$$

$$p_{xLD2} = \sigma, \tag{91}$$

$$\frac{\partial u_{D2}}{\partial x_L} = \varepsilon, \tag{92}$$

$$p_{yLD2} = 0, \tag{93}$$

$$d\psi_2 = dz. \tag{94}$$

The components of (82) are determined as written below.

$$u_{0D3} = \int \sigma_{B2B3h1} d\varepsilon_{B2B3h1}, \tag{95}$$

$$\alpha_{D3} = -1, \tag{96}$$

$$p_{xLD3} = -\sigma_{B2B3h1}, \tag{97}$$

$$\frac{\partial u_{D3}}{\partial x_L} = \varepsilon_{B2B3h1}, \tag{98}$$

$$p_{yLD3} = 0, \tag{99}$$

$$d\psi_3 = -dz_1. \tag{100}$$

The integrals (80), (81) and (82) are solved by the MatLab. The *J* is found by inserting (80), (81) and (82) in (79). Since the value of *J* matches the SERR, it can be concluded that the analysis is correct.

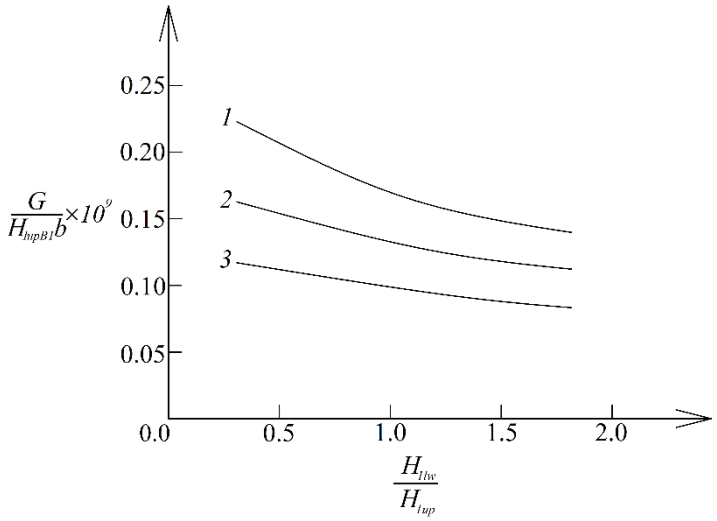

Fig. 3 The SERR - H_{1lw}/H_{1up} graphs (1 - at $H_{1lwB3}/H_{1lwB1} = 0.5$, 2 - at $H_{1lwB3}/H_{1lwB1} = 1.0$ and 3 - at $H_{1lwB3}/H_{1lwB1} = 2.0$)

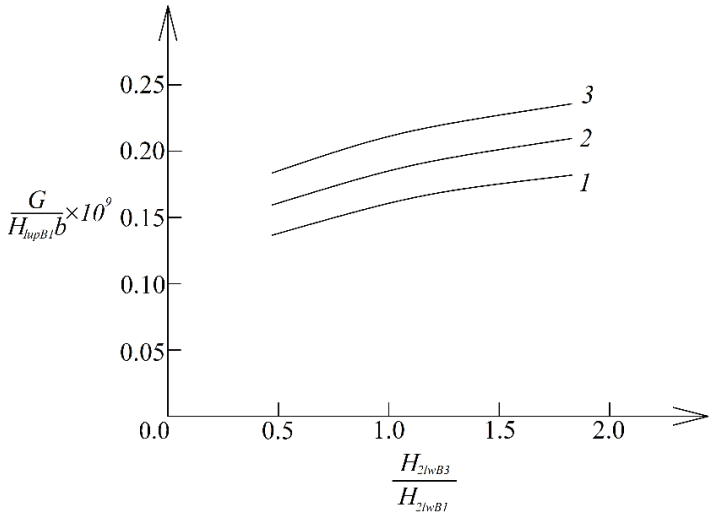

Fig. 4 The SERR - H_{2lwB3}/H_{2lwB1} graphs (1-at $H_{2lw}/H_{2up} = 0.5$, 2 - at $H_{2lw}/H_{2up} = 1.0$ and 3-at $H_{2lw}/H_{2up} = 2.0$)

4. Results and discussion

The change of the SERR when the parameters of the model are varied is studies next.

The following data are used: $b = 0.020$ m, $l = 0.600$ m, $h = 0.030$ m, $a = 0.300$ m, $\beta = 0.0025$ 1/s^2, $m = 2$ kg, $\rho_i = 0.6$ (here, $i = 1,2,\ldots,7$) and $\mu_i = 0.7$ (here, $i = 1,2,\ldots,14$). The findings are illustrated by various graphs.

The graphs in Fig. 3 reveal the change of the SERR due to variation of H_{1lw}/H_{1up} and H_{1lwB3}/H_{1lwB1} ratios.

The SERR is presented in Fig. 3 in normalized form by the formula $G/(H_{1upB1}b)$.

The graphs indicate a continuous reduction of the SERR as a result of increase of H_{1lw}/H_{1up} and H_{1lwB3}/H_{1lwB1} ratios (Fig. 3).

Opposite behaviour, i.e., continuous growth of the SERR can be seen in Fig. 4 where the effects of the variation of H_{2lw}/H_{2up} and H_{2lwB3}/H_{2lwB1} ratios are illustrated.

The growth of the SERR in Fig. 4 can be explained by reduction of the rod stiffness due to increase of H_2.

A similar kind of behaviour, i.e., growth of the SERR can be observed also in Fig. 5 where the findings about the influence of the variation of H_{3lw}/H_{3up} and H_{3lwB3}/H_{3lwB1} ratios are presented.

The graphs displayed in Fig. 6 indicate that the SERR decreases with increasing of n_{lw}/n_{up} ratio. Decreasing of the SERR is seen also with increasing of n_{lwB3}/n_{lwB1} ratio (Fig. 6).

Fig. 7 shows the results about the change of the SERR with increase of r_{lwB3}/r_{lwB1} ratio for different r_{lw}/r_{up} ratios. The graphs indicate decreasing of the SERR (Fig. 7).

The approach developed in this paper can be applied also for checking the safety of a functionally graded non-linear viscoelastic rod in which a longitudinal crack is observed during lifetime. For instance, the approach can be used to check at what values of the parameter, β, that governs the rotation of the rod crack propagation will not initiate. For this purpose, the variation of

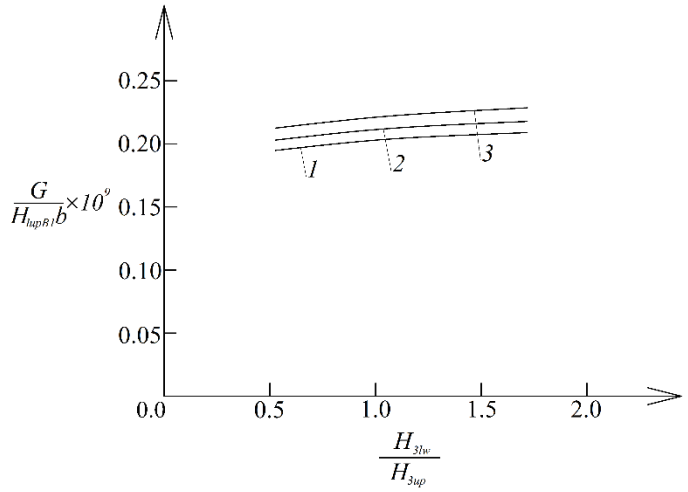

Fig. 5 The SERR - H_{3lw}/H_{3up} graphs (1 - at $H_{3lwB3}/H_{3lwB1} = 0.5$, 2 - at $H_{3lwB3}/H_{3lwB1} = 1.0$ and 3 - at $H_{3lwB3}/H_{3lwB1} = 2.0$)

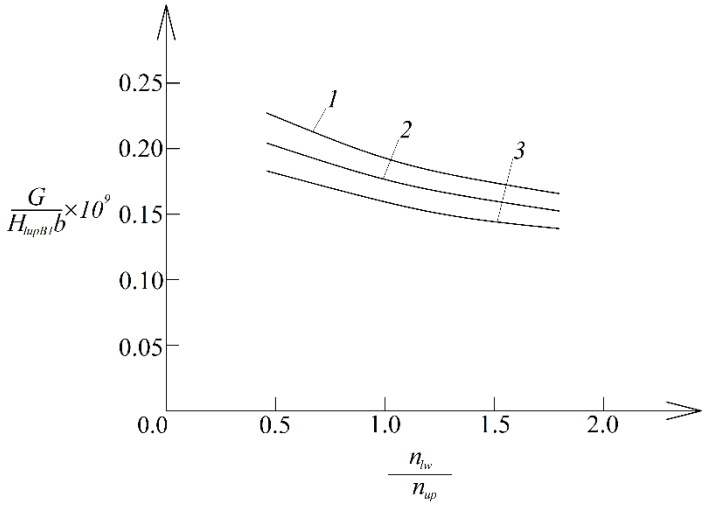

Fig. 6 The SERR - n_{lw}/n_{up} graphs (1-at $n_{lwB3}/n_{lwB1} = 0.5$, 2-at $n_{lwB3}/n_{lwB1} = 1.0$ and 3-at $n_{lwB3}/n_{lwB1} = 2.0$)

the SERR induced by increase of β has to be analyzed. The graph of this variation is reported in Fig. 8. The value of β at which the SERR reaches the fracture toughness, G_C, is the boundary value denoted by β_{lmt} in Fig. 8 (the fracture toughness is a parameter defined as the SERR at the initiation of crack propagation). At $\beta < \beta_{lmt}$ crack propagation will not initiate (in this sense the safety of the rod against crack propagation is guaranteed).

The approach can be applied to determine the boundary length of the crack (this is the length at which crack propagation initiates). Determination of the boundary crack length is demonstrated in Fig. 9 where the variation of the SERR with increase of a/l ratio is presented. The boundary crack length corresponds to the fracture toughness as displayed in Fig. 9.

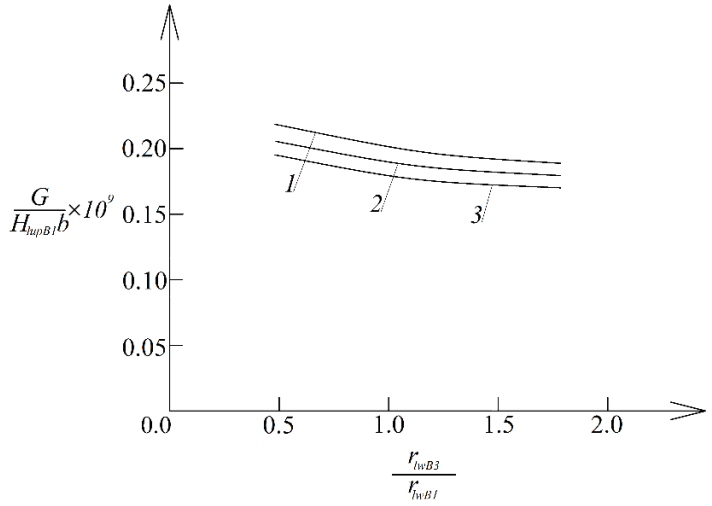

Fig. 7 The SERR-r_{lwB3}/r_{lwB1} graphs (1-at $r_{lw}/r_{up} = 0.5$, 2-at $r_{lw}/r_{up} = 1.0$ and 3-at $r_{lw}/r_{up} = 2.0$)

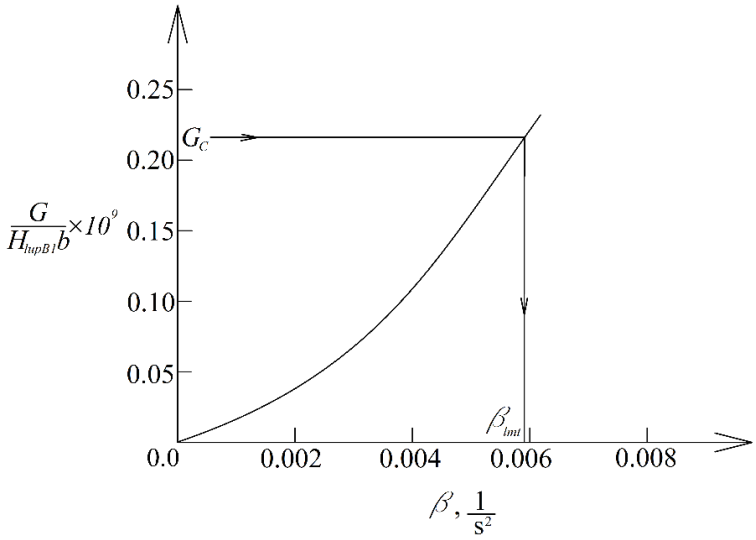

Fig. 8 The SERR-β graph

If the crack length does not exceed its boundary value crack propagation will not initiate and the safety of the rod is guarantied.

5. Conclusions

An approach for analyzing longitudinal fracture in non-linear viscoelastic rods performing non-uniform rotational movement is developed. The rods are functionally graded along thickness and length. First, a general treatment of the problem is presented. Determination of the forces of inertia and their distribution along the length of a rod hosting a longitudinal crack is considered in detail.

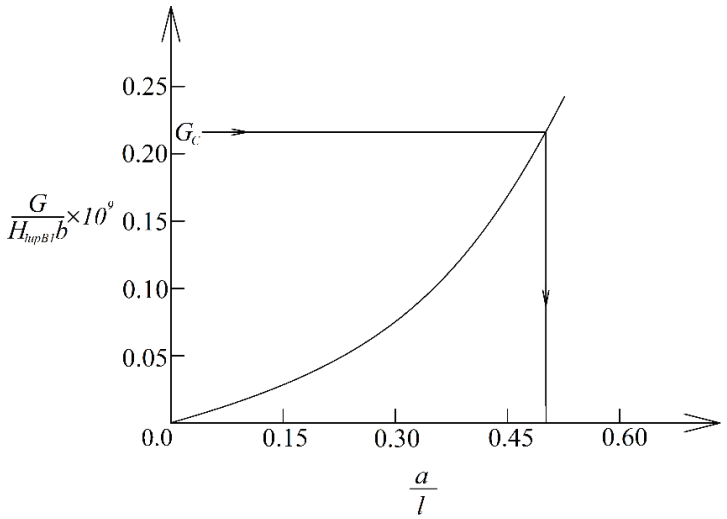

Fig. 9 The SERR-a/l ratio graph

A general approach for deriving the SERR under action of the forces of inertia is reported for an arbitrary law of rotation of the rod. Then the general approach is applied for a particular case. The correctness of the SERR solution is confirmed by using the integral *J*. The change of the SERR due to variation of various parameters of the theoretical model of a rod performing non-uniform rotation is thoroughly studied. The results are displayed in a variety of graphs. It is found that increase of H_{1lw}/H_{1up}, H_{1lwB3}/H_{1lwB1}, n_{lw}/n_{up}, n_{lwB3}/n_{lwB1}, r_{lwB3}/r_{lwB1} and r_{lw}/r_{up} ratios is accompanied by reduction of the SERR. The analysis indicates that the effect of variation of H_{1lw}/H_{1up}, H_{1lwB3}/H_{1lwB1} ratios on the SERR is stronger than the effect of variation n_{lw}/n_{up}, n_{lwB3}/n_{lwB1}, r_{lwB3}/r_{lwB1} and r_{lw}/r_{up} ratios in sense that the SERR- H_{1lw}/H_{1up} curves are stepper and the distance between these curves at different H_{1lwB3}/H_{1lwB1} ratios is bigger. The increase of H_{2lw}/H_{2up}, H_{2lwB3}/H_{2lwB1}, H_{3lw}/H_{3up} and H_{3lwB3}/H_{3lwB1} ratios generate growth of the SERR (here, the effect of variation of H_{2lw}/H_{2up} and H_{2lwB3}/H_{2lwB1} ratios is stronger than the effect of H_{3lw}/H_{3up} and H_{3lwB3}/H_{3lwB1} ratios). It is demonstrated that the approach can be applied also for checking the safety of rods in which a longitudinal crack is observed during lifetime. For instance, it is shown that the approach can be used for determining the boundary value of the parameter governing the rotation of the rot and the boundary crack length (the rod can be regarded as safe if the parameter involved in the law of rotation and the crack length do not exceed their boundary values). The paper contributes for clarifying the longitudinal facture in rods performing non-uniform rotation and helps for improving their safety.

References

Akbaş, Ş.D., Ersoy, H., Akgöz, B. and Civalek, Ö. (2021), "Dynamic analysis of a fiber-reinforced composite beam under a moving load by the Ritz method", *Math.*, **9**(9), 1048. https://doi.org/10.3390/math9091048.

Amara, K., Bouazza, M. and Fouad, B. (2016), "Postbuckling analysis of functionally graded beams using

nonlinear model", *Periodica Polytechnica Mech. Eng.*, **60**(2), 121-128. https://doi.org/10.3311/PPme.8854.

Atmane, H.A., Bedia, E.A.A., Bouazza, M., Tounsi, A. and Fekrar, A. (2016), "On the thermal buckling of simply supported rectangular plates made of a sigmoid functionally graded Al/Al2O3 based material", *Mech. Solid.*, **51**, 177-187. https://doi.org/10.3103/S0025654416020059.

Bouazza, M. and Zenkour, A.M. (2020), "Vibration of carbon nanotube-reinforced plates via refined *n*th-higher-order theory", *Arch. Appl. Mech.*, **90**, 1755-1769. https://doi.org/10.1007/s00419-020-01694-3.

Bouazza, M., Zenkour, A.M. and Benseddiq, N. (2018), "Effect of material composition on bending analysis of FG plates via a two-variable refined hyperbolic theory", *Arch. Mech.*, **70**(2), 1-23.

Broek, D. (1986), *Elementary Engineering Fracture Mechanics*, Springer.

Civalek, Ö., Akbas, S.D., Akgöz, B. and Dastjerdi, S. (2021), "Forced vibration analysis of composite beams reinforced by carbon nanotubes", *Nanomater.*, **11**, 571. https://doi.org/10.3390/nano 11030571.

Dastjerdi, S., Akgöz, B., Civalek, Ö., Malikan, M. and Eremeyev, V.A. (2020), "On the non-linear dynamics of torus-shaped and cylindrical shell structures", *Int. J. Eng. Sci.*, **156**, 103371. https://doi.org/10.1016/j.ijengsci.2020.103371.

Derbale, A., Bouazza, M. and Benseddiq, N. (2021), "Analysis of the mechanical and thermal buckling of laminated beams by new refined shear deformation theory", *Iran. J. Sci. Technol. Trans. Civil Eng.*, **45**, 89-98. https://doi.org/10.1007/s40996-020-00417-6.

Dolgov, N.A. (2005), "Determination of stresses in a two-layer coating", *Strength Mater.*, **37**(2), 422-431. https://doi.org/10.1007/s11223-005-0053-7.

Dolgov, N.A. (2016), "Analytical methods to determine the stress state in the substrate-coating system under mechanical loads", *Strength Mater.*, **48**(1), 658-667. https://doi.org/10.1007/s11223-016-9809-5.

Dowling, N.E. (2013), *Mechanical Behaviour of Materials*, Person.

El-Galy, I.M., Saleh, B.I. and Ahmed, M.H. (2019), "Functionally graded materials classifications and development trends from industrial point of view", *SN Appl. Sci.*, **1**, 1378. https://doi.org/10.1007/s42452-019-1413-4.

Ellali, M., Alazwari, M.A., Bouazza, M., Eltaher, M.E. and Benseddiq, N. (2024), "Effects of changing materials properties for vibration of FGM beam using integral shear deformation model", *Couple. Syst. Mech.***, 13**, 277-291. https://doi.org/10.12989/csm.2024.13.4.277.

Ellali, M., Amara, K. and Bouazza, M. (2024), "Thermal buckling of porous FGM plate integrated surface-bonded piezoelectric", *Couple. Syst. Mech.***, 13**(2), 171-186. https://doi.org/10.12989/csm.2024.13.2.171.

Ellali, M., Bouazza, M. and Amara, K. (2022), "Thermal buckling of a sandwich beam attached with piezoelectric layers via the shear deformation theory", *Arch. Appl. Mech.*, **92**, 657-665. https://doi.org/10.1007/s00419-021-02094-x.

Ellali, M., Bouazza, M. and Zenkour, A.M. (2022), "Impact of micromechanical approaches on wave propagation of FG plates via indeterminate integral variables with a hyperbolic secant shear model", *Int. J. Comput. Meth.*, **19**(9), 2250019. https://doi.org/10.1142/S0219876222500190.

Ellali, M., Bouazza, M. and Zenkour, A.M. (2023), "Wave propagation of FGM plate via new integral inverse cotangential shear model with temperature-dependent material properties", *Geomech. Eng.*, **33**, 427-437. https://doi.org/10.12989/gae.2023.33.5.427.

Ellali, M., Bouazza, M. and Zenkour, A.M. (2024), "Hygrothermal vibration of FG nanobeam via nonlocal unknown integral variables secant-tangential shear deformation coupled theory with temperature-dependent material properties", *Eur. J. Mech.-A/Solid.*, **105**, 105243. https://doi.org/10.1016/j.euromechsol.2024.105243.

Faleh, N.M., Ahmed, R.A. and Fenjan, R.M. (2018), "On vibrations of porous FG nanoshells", *Int. J. Eng. Sci.*, **133,** 1-14. https://doi.org/10.1016/j.ijengsci.2018.08.007.

Gasik, M.M. (2010), "Functionally graded materials: bulk processing techniques", *Int. J. Mater. Prod. Technol.*, **39**(1-2), 20-29. https://doi.org/10.1504/IJMPT.2010.034257.

Hedia, H.S., Aldousari, S.M., Abdellatif, A.K. and Fouda, N.A. (2014), "New design of cemented stem using functionally graded materials *(FGM)*", *Biomed. Mater. Eng.*, **24**(3), 1575-1588. https://doi.org/10.3233/BME-140962.

Mahamood, R.M. and Akinlabi, E.T. (2017), *Functionally Graded Materials*, Springer.
Markworth, A.J., Ramesh, K.S. and Parks, Jr. W.P. (1995), "Review: Modeling studies applied to functionally graded materials", *J. Mater. Sci.*, **30**(3), 2183-2193. https://doi.org/10.1007/BF01184560.
Miyamoto, Y., Kaysser, W.A., Rabin, B.H., Kawasaki, A. and Ford, R.G. (1999), *Functionally Graded Materials: Design, Processing and Applications*, Kluwer Academic Publishers, Dordrecht/London/Boston.
Nemat-Allal, M.M., Ata, M.H., Bayoumi, M.R. and Khair-Eldeen, W. (2011), "Powder metallurgical fabrication and microstructural investigations of Aluminum/Steel functionally graded material", *Mater. Sci. Appl.*, **2**(5), 1708-1718. https://doi.org/10.4236/msa.2011.212228.
Rizov, V.I. (2020), "Analysis of two lengthwise cracks in a viscoelastic inhomogeneous beam structure", *Eng. Trans.*, **68**, 397-415. https://doi.org/10.24423/EngTrans.1214.20201125.
Rizov, V.I. (2022), "Effects of periodic loading on longitudinal fracture in viscoelastic functionally graded beam structures", *J. Appl. Comput. Mech.*, **8**(1), 370-378. https://doi.org/10.22055/JACM.2021.37953.3141.
Rizov, V.I. (2024), "The effect of delamination between layers in U-shaped members made of functionally graded multilayered viscoelastic materials", *J. Appl. Comput. Mech.*, **10**, 830-841. https://doi.org/10.22055/jacm.2024.46014.4449.
Rizov, V.I. and Altenbach, H. (2019), "Application of the classical beam theory for studying lengthwise fracture of functionally graded beams", *Technische Mechanik*, **39**(2), 229-240. https://doi.org/10.24352/UB.OVGU-2019-021.
Rizov, V.I. and Altenbach, H. (2019), "On the analysis of lengthwise fracture of functionally graded round bars", *Struct. Integr. Life*, **19**(2), 102-108.
Rizov, V.I. and Altenbach, H. (2022), "Multilayered non-linear viscoelastic beams subjected to torsion at a constant speed: a delamination analysis", *Eng. Ttrans.*, **70**(1), 53-66. https://doi.org/10.24423/EngTrans.1720.20220303.
Saiyathibrahim, A., Subramaniyan, R. and Dhanapl, P. (2016), "Centrefugally cast functionally graded materials-review", *International Conference on Systems, Science, Control, Communications, Engineering and Technology*, 68-73.
Shrikantha Rao, S. and Gangadharan, K.V. (2014), "Functionally graded composite materials: an overview", *Procedia Mater. Sci.*, **5**(1), 1291-1299. https://doi.org/10.1016/j.mspro.2014.07.442.
Tokovyy, Y. (2019), "Solutions of axisymmetric problems of elasticity and thermoelasticity for an inhomogeneous space and a half space", *J. Math. Sci.*, **240**(1), 86-97. https://doi.org/10.1007/s10958-019-04337-3.
Tokovyy, Y. and Ma, C.C. (2017), "Three-dimensional elastic analysis of transversely-isotropic composites", *J. Mech.*, **33**(6), 821-830. https://doi.org/10.1017/jmech.2017.91.
Tokovyy, Y. and Ma, C.C. (2019), "Elastic analysis of inhomogeneous solids: History and development in brief", *J. Mech.*, **18** (1), 1-14. https://doi.org/10.1017/jmech.2018.57.
Tokovyy, Y. and Ma, C.C. (2021), *The Direct Integration Method for Elastic Analysis of Nonhomogeneous Solids*, Cambridge Scholars Publishing.
Tokovyy, Y.V. (2023), "Elastic and thermoelastic response of multilayer inhomogeneous hollow cylinders", *Mech. Adv. Mater. Struct.*, **31**(17), 3889-3901. https://doi.org/10.1080/15376494.2023.2186548.
Toudehdehghan, J., Lim, W., Foo1, K.E., Ma'arof, M.I.N. and Mathews, J. (2017), "A brief review of functionally graded materials", *MATEC Web Conf.*, **131**, 03010. https://doi.org/10.1051/matecconf/201713103010UTP-UMP.
Varbanov, Chr., Tepavicharov, A. and Ganev, T. (1992), *Applied Theory of Elasticity and Plasticity*, Technique.
Yıldırım, A. and Akgöz, B. (2024), "Buckling behavior of nickel microbeams based on reformulated strain gradient theory", *Appl. Phys. A*, **130**, 832. https://doi.org/10.1007/s00339-024-08013-5.